


Article

Performance Evaluation of Reinforced Recycled Aggregate Concrete Columns under Cyclic Loadings

Fan Wang ¹, Yong Yu ¹ , Xin-Yu Zhao ^{1,*}, Jin-Jun Xu ^{2,*}, Tian-Yu Xie ³ and Simret Tesfaye Deresa ²

¹ State Key Laboratory of Subtropical Building Science, South China University of Technology, Guangzhou 510640, China; wangfan@scut.edu.cn (F.W.); yuyong1990@foxmail.com (Y.Y.)

² College of Civil Engineering, Nanjing Technology University, Nanjing 210023, China; simtes2009@gmail.com

³ School of Civil, Environmental and Mining Engineering, University of Adelaide, Adelaide 5005, Australia; tianyu.xie@adelaide.edu.au

* Correspondence: ctzhaoxy@scut.edu.cn (X.-Y.Z.); jjxu_concrete@163.com (J.-J.X.)

Received: 26 February 2019; Accepted: 28 March 2019; Published: 8 April 2019



Abstract: Recycled concrete aggregates (RCAs) generated from construction and demolition activities have been recognized as a feasible alternative to natural aggregates (NAs). Naturally, the columns fabricated with reinforced recycled concrete (RRC) have been proposed and investigated to promote the structural use of recycled aggregate concrete (RAC). There is still, however, very limited modeling research available to reproduce, accurately and efficiently, the seismic response of RRC columns under lateral cyclic loading; proper evaluations are also lacking on addressing the columns' seismic behaviors. To fill some of those research gaps, a fiber-based numerical model is developed in this study and then validated with the experimental results published in the literature. Subsequently, the numerical model justified is applied to carry out a comprehensive parametric study to examine the effects of a range of variables on the hysteretic characteristics of RRC columns. Furthermore, a grey relational analysis is conducted to establish quantifiable evidence of key variable sensitivities. The evaluation results imply that the use of the additional water method (AWM) for manufacturing RAC is likely to reduce the lateral load-carrying capacity of the RRC columns (up to 10%), whereas the opposite would occur if a conventional mixing procedure is adopted. Moreover, compared with other factors such as steel area ratio, the content of RCA replacement has a less remarkable effect on the seismic performance of the RRC columns. In general, the RRC columns possess acceptable seismic-resistant properties, and they can be used in earthquake-prone regions with confidence.

Keywords: reinforced concrete; recycled aggregate concrete; columns; seismic performance; numerical analysis; variable sensitivity

1. Introduction

Recycled concrete aggregates (RCAs) generated from construction and demolition waste (CDW) have been deemed as a potential alternative to natural aggregates (NAs) with the advantage of minimizing the environmental impacts of CDW [1–4], where the resulting concrete products, termed recycled aggregate concrete (RAC), are now received as a type of “green concrete” [5–10]. Along this line, the reinforced recycled concrete (RRC) members (i.e., reinforced concrete slabs, beams, columns and shear walls manufactured with RCAs) have been developed and explored to promote the sustainable use of RAC at the structural level.

Research efforts have been dedicated to characterizing the properties of RRC beams and columns in static loading conditions. The influence of RCAs on the monotonic shear [11–23] or flexural [24–35] behaviors of RRC beams has also been extensively experimentally investigated, with the replacement

ratio (i.e., r) varied from 0% to 100%. The experimental outcomes indicate that: (i) in either shear or flexural failure, the presence of various RCA replacement ratios only has a limited influence on the damage process and failure pattern of RRC beams; (ii) an increased replacement ratio appears to reduce the load-carrying capacity of RRC beams. It should be highlighted that the RCAs used in the aforementioned studies were generally not treated before concreting. For the purpose of improving the performance of RCAs, Katkhuda and Shatarat [36] adopted an acid treatment to eliminate the weak layer resulting from the adhesive mortar on RCAs so as to enhance the behavior of RRC beams.

In the case of RRC columns, similar findings have been reported in a number of compression tests using untreated RCAs [37–39]: (i) RCA replacement ratio had no remarkable influence on the failure progression of the columns, and (ii) the compressive strength and the elastic stiffness of RRC columns were generally lower than those of conventional RC columns made with NAs, where the reductions in these properties depended on the RCA content.

It is noteworthy that two thorough review studies by Silva et al. [40] and Tošić et al. [41] have clearly shown that the design code Eurocode 2 can provide a good prediction for the load-carrying capacity of RRC beams without stirrups. However, for the beams with stirrups, which are more significant in practice—the predictions by Eurocode 2 showed a remarkable gap compared to the measurements, suggesting that the underlying mechanisms still needed to be revealed towards more reliable designs.

Up to now, however, research is still scarce on the feasibility of using RAC in concrete elements designed with seismic-resistant purposes. Only a few experimental studies have been conducted aiming to clarify the effect of the incorporation of RCA on the seismic response of RRC columns. Xiao et al. [42] and Yang [43] investigated the cyclic behaviors of RRC columns subjected to axial compression and lateral load reversals. They observed that an increased RCA replacement ratio tended to reduce the lateral load resistance of RRC columns. Moreover, both ductility and energy-dissipating capacities of RRC columns declined to an extent, owing to the incorporation of RCA.

Seismic modeling is essential to generalize the experimental outcomes of RRC columns so as to gain the confidence of their structural use in seismic regions. Again, it is not surprising that only very few studies have been conducted on that important issue. Xiao et al. [44] have numerically modeled a three-dimensional RAC test frame in the OpenSees platform and validated that fiber-based finite elements can be used to approximate the seismic response of RRC frame structures. Still, the potential influences of the unique material properties of RAC on the RRC columns have not yet been numerically and systematically studied.

Thus, the main purposes of the present study are two-fold: (i) to investigate the modeling method of RRC columns under combined action of constant axial load and cyclic lateral loading, based upon a fiber-based numerical approach; (ii) to examine the effects of a range of variables (such as the replacement ratio of RCAs, the mixing method of RAC, and the yield strength and area ratio of longitudinal reinforcing bars) on the seismic performance of RRC columns. This allows an insightful seismic evaluation of those columns that has been less often addressed before.

The remainder of this paper is organized as follows: a fiber-based modeling method is firstly developed to reproduce the cyclic response of RRC columns. Upon a careful benchmarking, the model is employed to perform a comprehensive parametric investigation to examine the effects of a set of potential influencing variables on the seismic performances of RRC columns. Furthermore, a grey relational model, capable of detecting the underlying, not easily discernible tendencies, is used to study the sensitivity of key variables. The research outcomes presented in this study provides valuable insights on the seismic design of RRC columns. The outcomes can be easily extended to performance-based evaluations, hence they are beneficial to the safe and rational use of those columns as lateral-load-resisting elements.

2. Numerical Modelling

2.1. Description of the Modeling Method

A fiber beam model based primarily on the section discretization into fibers was used in this study to predict the hysteretic response of RRC columns subject to lateral cyclic loadings. The SeismoStruct software [45] was employed as the platform to implement the model. A cantilever-type column (i.e., the column's lower end is fixed while the top end is free) was modeled in order to simulate the boundary conditions commonly adopted in column cyclic tests (see Figure 1).

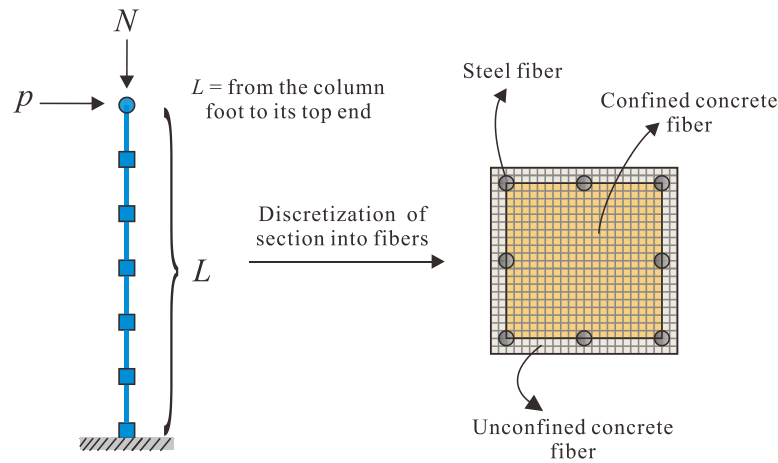


Figure 1. Loading scheme, boundary conditions, and fiber discretization for reinforced recycled concrete (RRC) columns.

The element type “inelastic displacement-based frame element” provided in SeismoStruct was chosen, which was capable of accounting for both material and geometric nonlinearities accurately. It assumed that the concrete and steel bars were rigidly connected, since Zhang et al. [46] have clearly concluded that the bond-slip effect on the flexure-controlled RC columns was generally insignificant. Only flexural bending failure was considered in the proposed model, because such a failure is typical for slender or well-reinforced RC columns [47–51]. Coping with column shear failure was, thus, out of the scope of this study.

2.1.1. Constitutive Model for Recycled Aggregate Concrete (RAC)

The “con_ma” model [52–54] available in SeismoStruct was used to represent the uniaxial constitutive behavior of RAC. This model can be completely determined by the following three key properties: the elastic modulus (E_c), the cylindrical compressive strength (f_c), and the peak strain (ϵ_{co}^r). Based on a thorough review and extensive experimental database of RAC, Gholampour et al. [55] have proposed an accurate stress–strain relationship for obtaining f_c and E_c of RAC:

$$f_c(\text{MPa}) = \frac{23.5 \times 0.998^r \times (w_{\text{eff}}/c + 0.09)}{w_{\text{eff}}/c^{1.7}}, \quad (1)$$

$$E_c(\text{GPa}) = 0.016 \times (6.1 - 0.015r) \times (5.3 - 1.7w_{\text{eff}}/c)^{3.9}, \quad (2)$$

where r = the replacement ratio of RCAs ($0\% \leq r \leq 100\%$), and w_{eff}/c = the effective water-to-cement ratio ($0.3 \leq w_{\text{eff}}/c \leq 0.8$).

Xiao et al. [56] suggested an equation to determine the peak strain of RAC (ϵ_{co}^r) as a function of r :

$$\epsilon_{co}^r = \epsilon_{co}^n \left(1 + \frac{r}{65.715r^2 - 109.43r + 48.989} \right). \quad (3)$$

The value of ε_{co}^n in the above equation was determined based on the work by Lim and Ozbakkaloglu [57]:

$$\varepsilon_{co}^n = \frac{f_c^{0.225w_d}}{1000} w_s w_a; w_d = \left(\frac{2400}{\rho_{c,f}} \right)^{0.45}; w_s = \left(\frac{152}{D_c} \right)^{0.1}; w_a = \left(\frac{2D_c}{H_c} \right)^{0.13}, \quad (4)$$

where $\rho_{c,f}$ = the bulk density of concrete ($2250 \text{ kg/m}^3 \leq \rho_{c,f} \leq 2550 \text{ kg/m}^3$); D_c and H_c = the diameter and height of cylinder concrete samples, respectively ($50 \text{ mm} \leq D_c \leq 400 \text{ mm}$, $100 \text{ mm} \leq H_c \leq 850 \text{ mm}$). w_d , w_s , and w_a are, respectively, the coefficients accounting for the concrete density and the samples' aspect ratio. It should be highlighted that $w_d = w_s = w_a = 1.0$ for the common NAC samples. Consequently $\rho_{c,f} = 2400 \text{ kg/m}^3$, $D_c = 152 \text{ mm}$, and $H_c/D_c = 2.0$.

2.1.2. Constitutive Model for Steel Reinforcement

The “stl_mp” model in SeismoStruct was used to describe the uniaxial tensile and compressive constitutive relationships of steel reinforcing bars. This model was initially proposed by Yassin [58], and then modified and extensively utilized by Menegotto-Pinto [59], Filippou et al. [60], and Monti [61]. For more details the reader can refer to the above articles.

2.2. Validation and Discussion

As discussed in Section 1, Xiao et al. [42] and Yang [43] have conducted cyclic tests on the seismic performance of RRC columns under constant axial load and cyclic lateral reversals. The loading process in the above experiments consisted of a load-controlled phase followed by a displacement-controlled phase. During the first phase, the lateral load was progressively exerted on the specimen with an of increment of, respectively, $0.20P_y$ [42] and 5 kN [43]. After steel yielded, the loading method was switched to the displacement-controlled mode. In both experiments the displacement increment was adopted as $1.0\Delta_y$ (Δ_y = the displacement at steel yielding). The loop at each drift level was repeated three times until the lateral load resistance dropped below 80% [42] or 70% [43] of the peak load. Figure 2 and Table 1 show the material properties and the geometries of the RRC cantilever-type test columns. Note that to compensate the larger water absorption of RAC, a so-called additional water method (AWM) (see Section 3.1 for detail) for RAC mix proportion was used in the aforementioned cyclic tests. The experimental outcomes from these tests were employed to validate the numerical model developed herein. The failure mode of all the test specimens was solely flexural-dominated failure (see Figure 3).

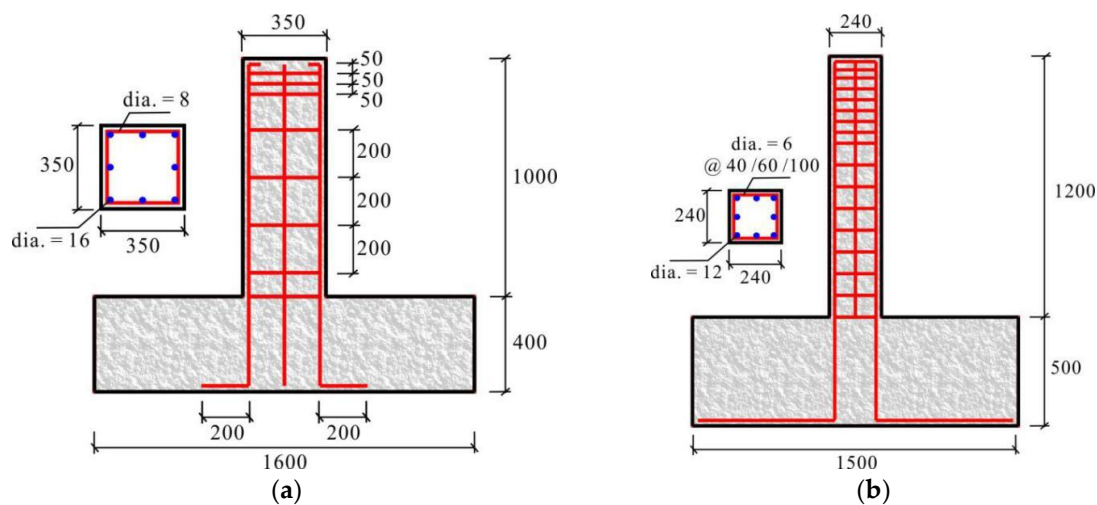


Figure 2. Reinforcement and geometry diagram of reported specimens (unit: mm). (a) Specimens in Xiao et al. [42], and (b) specimens in Yang [43].

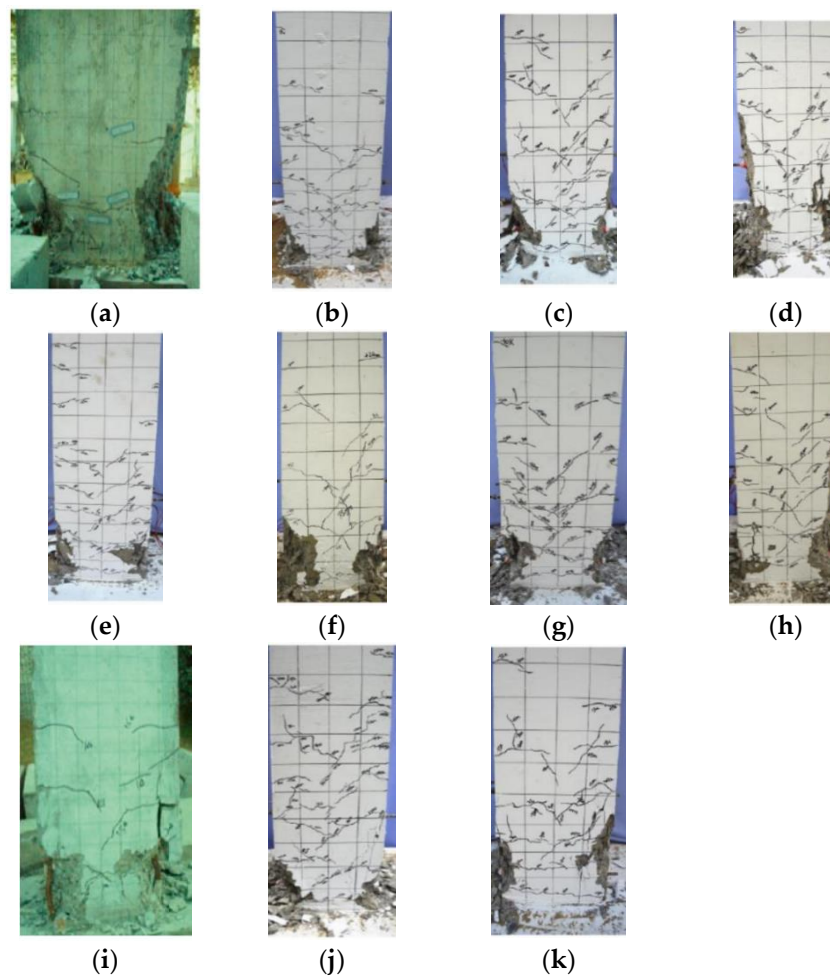


Figure 3. Flexural failure modes of test specimens. (a) NCCC-1 [42]; (b) NAC-0.30-40 [43]; (c) NAC-0.30-60 [43]; (d) NAC-0.30-100 [43]; (e) RAC50-0.30-40 [43]; (f) RAC50-0.30-60 [43]; (g) RAC50-0.30-100 [43]; (h) RAC100-0.30-60 [43]; (i) RCCC-2 [42]; (j) RAC50-0.15-60 [43]; and (k) RAC50-0.45-60 [43].

Following the modeling approach described previously, the global cyclic response of the specimens in [42,43] can be calculated. Figure 4 compares the lateral load-displacement hysteresis loops obtained from the experiments and the simulations.

Table 1. Experimental information of RRC specimens collected from literature.

Sample	w_{eff}/c	r [%]	f_c [MP]	E_c [GP]	L [mm]	$h = b$ [mm]	n	d [mm]	f_y [MP]	E_s [GP]	d_{hoop} [mm]	S [mm]	$f_{y,v}$ [MP]	$P_{u,t}$ [kN]	$P_{u,s}$ [kN]	$P_{u,t}/P_{u,s}$	μ_t	μ_s	μ_t/μ_s
Xiao et al. [42]																			
NCCC-1	0.488	0	28.98	36.3	1280	350	0.30	16	353	196	8	200	340	178	174	1.02	5.98	5.67	1.05
RCCC-2	0.43	100	26.98	25.0	1280	350	0.30	16	353	196	8	200	340	164	162	1.01	4.56	3.93	1.16
Yang [43]																			
NAC-0.30-40	0.45	0	33.52	33.0	1000	240	0.30	12	549	241	6	40	389	93	95	0.98	3.80	4.10	0.93
NAC-0.30-60	0.45	0	33.52	33.0	1000	240	0.30	12	549	241	6	60	389	92	94	0.98	3.63	3.94	0.92
NAC-0.30-100	0.45	0	33.52	33.0	1000	240	0.30	12	549	241	6	100	389	87	93	0.93	3.29	3.70	0.89
RAC50-0.30-40	0.45	50	28.88	31.6	1000	240	0.30	12	549	241	6	40	389	84	90	0.93	4.13	4.42	0.93
RAC50-0.30-60	0.45	50	28.88	31.6	1000	240	0.30	12	549	241	6	60	389	91	90	1.02	3.79	4.27	0.89
RAC50-0.30-100	0.45	50	28.88	31.6	1000	240	0.30	12	549	241	6	100	389	87	89	0.98	3.53	3.77	0.94
RAC50-0.15-60	0.45	50	28.88	31.6	1000	240	0.15	12	549	241	6	60	389	69	61	1.12	4.02	4.27	0.94
RAC50-0.45-60	0.45	50	28.88	31.6	1000	240	0.45	12	549	241	6	60	389	94	89	1.06	3.08	4.44	0.69
RAC100-0.30-60	0.45	100	28.00	31.3	1000	240	0.30	12	549	241	6	60	389	82	89	0.92	3.35	4.56	0.73
Average value																1.00			0.92
Cov																0.06			0.13

Note: Cov—Coefficient of variation.

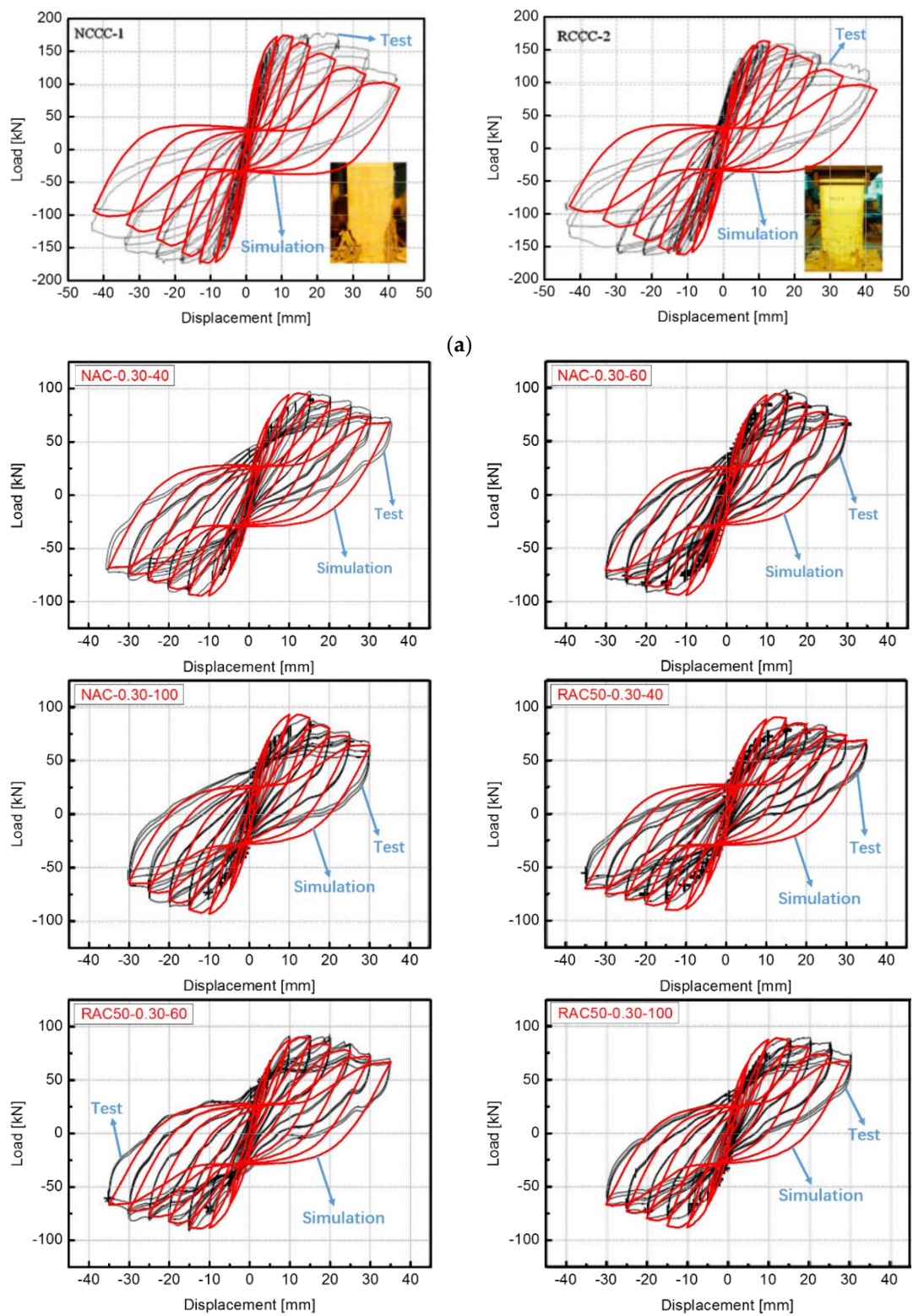


Figure 4. Cont.

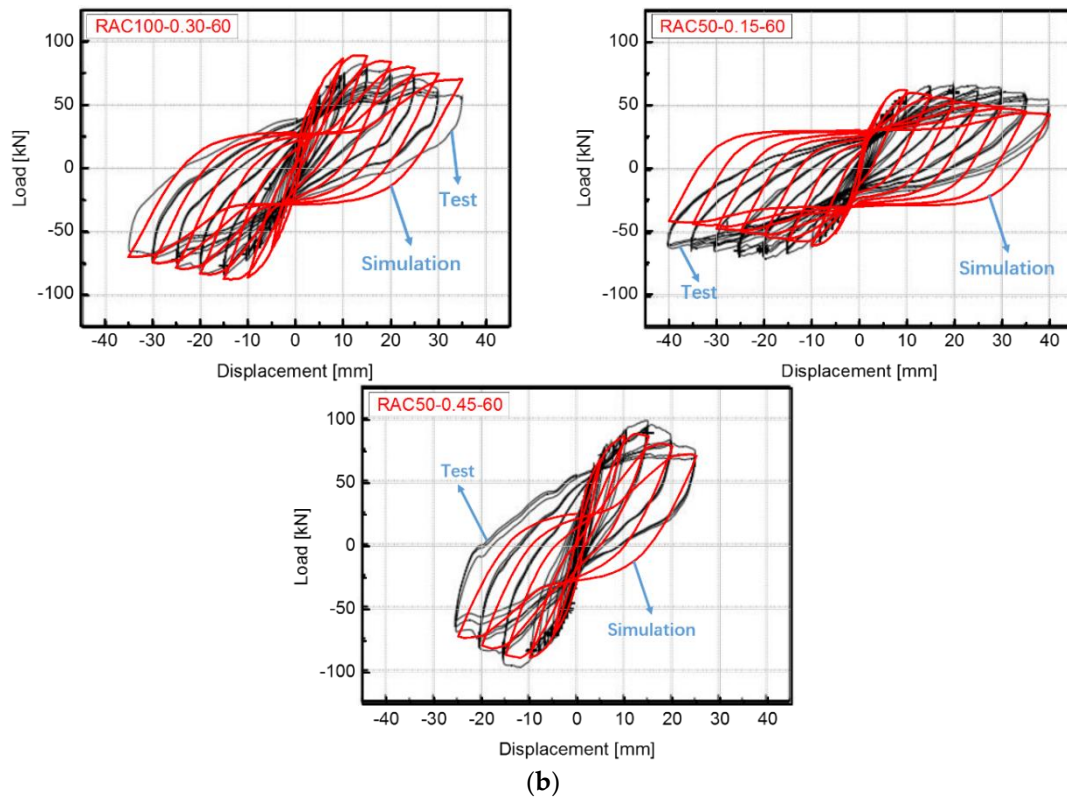


Figure 4. Comparison of hysteresis loops between experimental and numerical results. (a) Test specimens in Xiao et al. [42], and (b) test specimens in Yang [43].

The lateral load-carrying capacity and the ductility in Figure 4 were defined as the maximum lateral load (P_u) and the displacement ductility coefficient (μ), respectively. In Table 1, $P_{u,t}$ is the experimental ultimate load, $P_{u,s}$ is the corresponding numerical ultimate load, and μ_t and μ_s are the experimental and numerical displacement ductility coefficients, respectively. The value of μ is defined as the ratio of the ultimate lateral displacement (denoted as $\Delta_{0.85}$) at the load corresponding to 85% of the peak load in the descending backbone curve to the yield lateral displacement (denoted as Δ_y) determined based on the energy equivalence principle (see Figure 5).

$$\mu = \frac{\Delta_{0.85}}{\Delta_y} \quad (5)$$

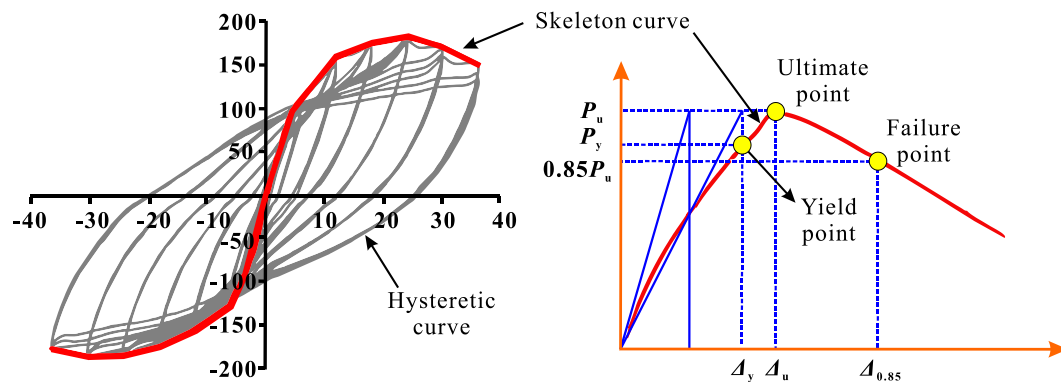


Figure 5. Load-displacement backbone curve.

From Figure 4 and Table 1, it is clear that the predicted hysteresis loops correlated well with the measured ones; the prediction-to-test ratio for the two major seismic performance indexes (P_u and μ) was close to unity ($P_{u,s}/P_{u,t} = 1.00$ and $\mu_s/\mu_t = 0.92$). It can also be seen that the coefficients of variation on the ultimate lateral load and displacement ductility were small on the whole. Hence, the finite-element model developed can provide an overall faithful tool to estimate the seismic performance of RRC columns.

3. Parametric Investigation

A parametric study was conducted so as to extrapolate the existing experimental outcomes for evaluating the seismic response of RRC columns. For convenience, the extended numerical models were established and discussed on the basis of the typical test columns in Yang [43] (i.e., NAC-0.30-60, RAC50-0.30-60, and RAC100-0.30-60; see Table 1). The numerical calculation was terminated once the lateral strength dropped to 70% of the peak strength in the descending branch, which was consistent with the loading protocol used in [43].

Four key variables were considered and varied in the parametric study: (1) the RCA percentage ($0\% \leq r \leq 100\%$), (2) the yield strength of longitudinal steel reinforcement ($300 \text{ MPa} \leq f_y \leq 500 \text{ MPa}$), (3) the area ratio of the steel ($1.57\% \leq \rho_s \leq 6.28\%$), and (4) bi-directional cyclic loading represented by the loading angle α ($0^\circ \leq \alpha \leq 45^\circ$).

The related properties for the numerical analyses were selected as (basically in accordance with [43]): (1) $b = h = 240 \text{ mm}$, $c = 25 \text{ mm}$, and $L = 1000 \text{ mm}$; (2) $f_y = 549 \text{ MPa}$, $f_{y,v} = 389 \text{ MPa}$, and $E_s = 241 \text{ GPa}$; (3) $d = 12 \text{ mm}$, $d_{\text{hoop}} = 6 \text{ mm}$, and $S = 60 \text{ mm}$; and (4) axial load ratio $n = 0.3$.

Note that the concrete mixing method was crucial to the mechanical properties of RAC. In view of this, two widely-accepted mixing methods—the additional water method (AWM) and the equivalent total water method (ETWM)—were considered in this numerical study. For each case studied, the following values of RCA replacement percentage were used: $r = 0\%$, 50% , or 100% , which corresponded, respectively, to the RAC's target strength $f_{c,0\%} = 33.52 \text{ MPa}$, $f_{c,50\%} = 28.88 \text{ MPa}$, or $f_{c,100\%} = 28.0 \text{ MPa}$, according to Yang [43].

It should be highlighted that the pre-saturation method may lead to inferior properties of RAC as compared to the AWM as a result of the bleeding effect. However, there are still different opinions. Ferreira et al. [62] have demonstrated that concrete mixes using the pre-saturation method exhibited slightly worse fresh and hardened state behaviors than mixes made with the AWM; however, the mechanical behavior differences observed were generally small and sometimes inconclusive. González-Taboada [63] have further clarified that this indeed depended on the water absorption of RCA: when the water absorption was low, both methods negatively affected concrete compressive strength, whereas when water absorption was high, compressive strength was not affected and both methods can be accurately used. The current authors also found that pre-saturation was, in general, similar to the AWM [64]. Therefore, regarding the AWM and pre-saturation methods, only the former was chosen to compare with the ETWM in this study.

3.1. Influences of r and of the Addition Water Method

Previous experimental investigations [62–75] have clearly reported that the mechanical properties of both RAC and the members containing RAC are predominated by the characteristics of RCAs (RCA percentage, the water absorption and density of RCAs, crushing damage in RCAs, etc.). Based on the water absorption capacity of RCAs, Xu et al. [64] suggested the underlying mechanism of strength reduction or enhancement of RAC manufactured with the AWM and ETWM mixing methods. Figure 6 illustrates the principle of strength variations on RAC determined by the two manufacturing methodologies: the AWM (i.e., [62,63,66]) and ETWM (i.e., [69–72]).

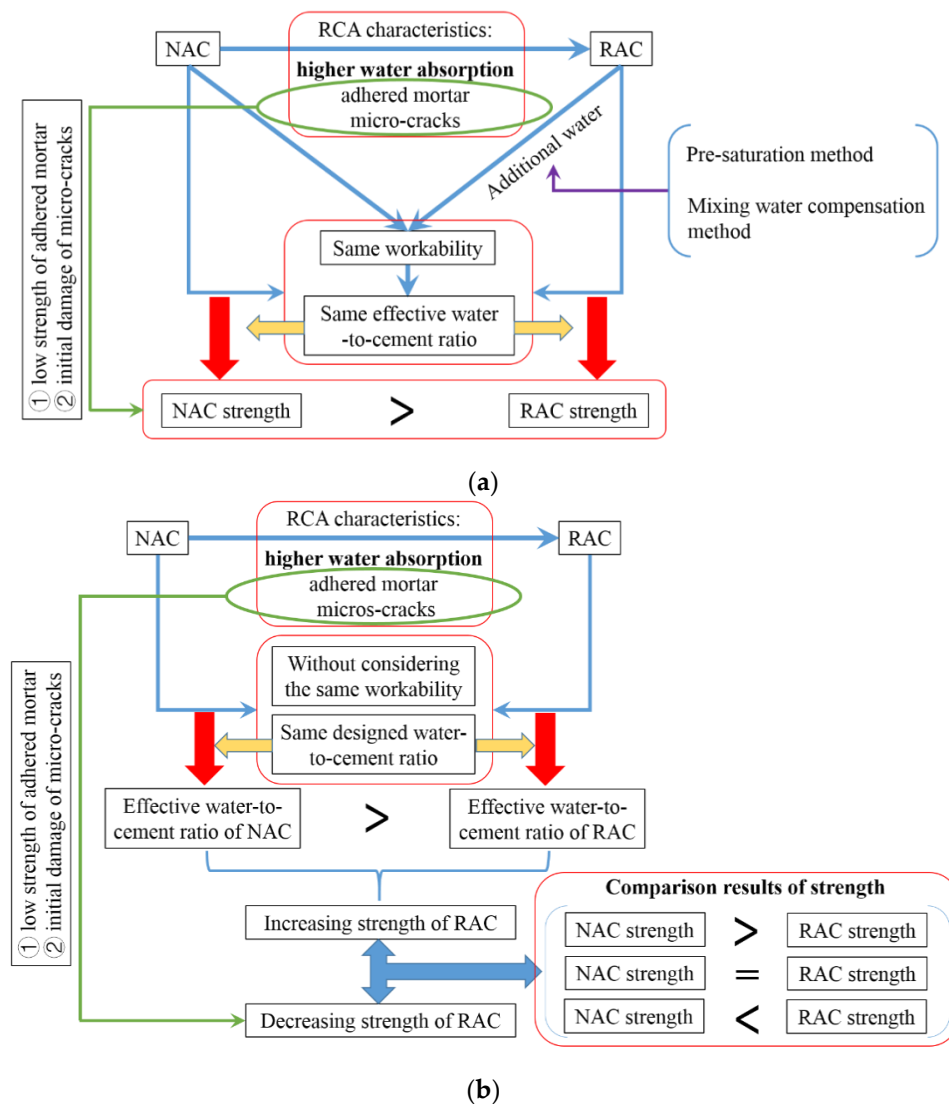


Figure 6. The relationship between recycled concrete aggregate (RCA) characteristics and concrete compressive strength using: (a) the additional water method, and (b) the equivalent total water method.

A careful inspection of compressive strength of RAC was carried out by examining the test results reported in Xiao et al. [56], Zega and Maio [76] (using AWM), as well as Chen et al. [73] (using ETWM). Figure 7 displays the compressive strength ratio of RAC with respect to that of an equivalent NAC versus the RCA content in light of the above works. It shows that an increase in the RCA percentage reduces the compressive strength ratio between RAC and NAC when the AWM is employed, whereas an increase in the RCA percentage results in an overall increase in the strength of RAC when the ETWM is otherwise used. These experimental results ascertain the principles of the equivalent effective water method and the equivalent total water method based on the way the method affects the relationship between the strengths of NAC and RAC (Figure 6).

In the present modeling, the RAC material properties were adopted from Xiao et al. [56] (in the case of the AWM) and Chen et al. [73] (the ETWM). Figures 8 and 9 show the predicted horizontal load-displacement hysteresis loops and seismic performance using different concrete mixing methods. It can be seen from Figures 8 and 9 that: (i) An increase in r resulted in an up to 10% decrease in P_u of RRC columns using the AWM, whereas the opposite occurred when the ETWM was adopted. However, (ii) the variation in P_u was generally lower than that of the f_c of RAC, consistently true for the two types of mixing methods. This was because the impacts of RCAs (i.e., low strength of adhered mortar and crushing damage in RCAs (i.e., [63–67])) could be largely reduced in RRC columns

as a result of structural effects such as the confinement provided by transverse steel reinforcement. Despite the above detrimental effects, (iii) the ductility of RRC columns manufactured with the AWM increased slightly with an increase in the ratio of RCA percentage, whereas for the ETWM no such obvious dependency on the replacement ratio could be found. This can be explained as the AWM may have led to a lower f_c compared to the ETWM, which in turn resulted in a decreasing brittleness [77].

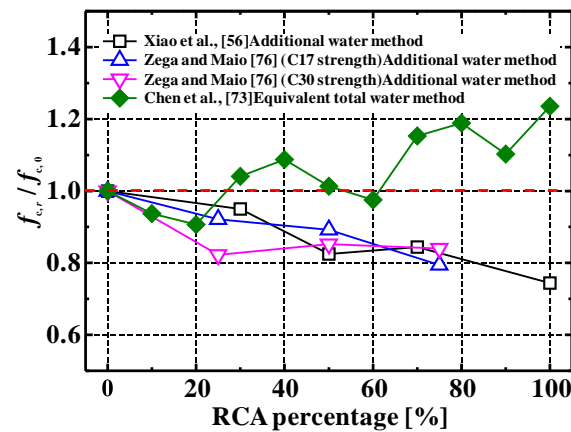


Figure 7. Effect of RCA percentage on 28-day compressive strength of recycled aggregate concrete (RAC) (Note: $f_{c,0}$ is the cylinder compressive strength when $r = 0\%$; $f_{c,r}$ is the cylinder compressive strength when $r \neq 0\%$).

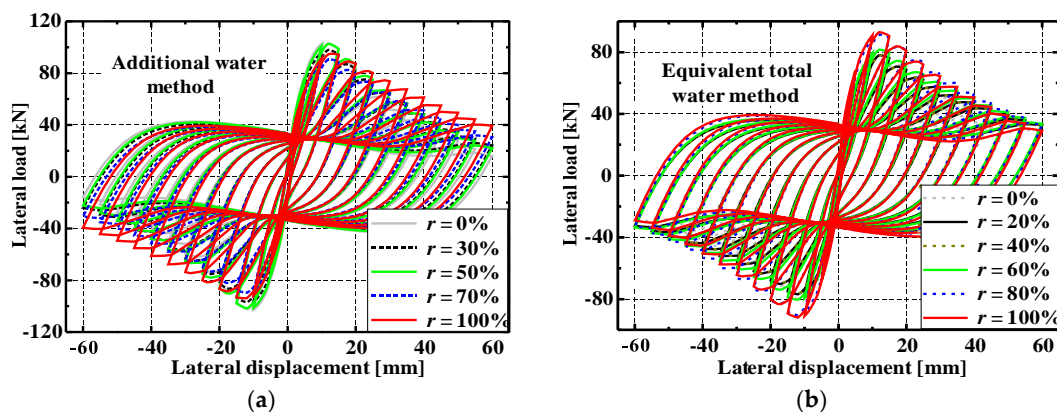


Figure 8. Effect of RCA percentage on hysteresis loops of RRC columns ($n = 0.3$). (a) Additional water method (Xiao et al. [56]). (b) Equivalent total water method (Chen et al. [72]).

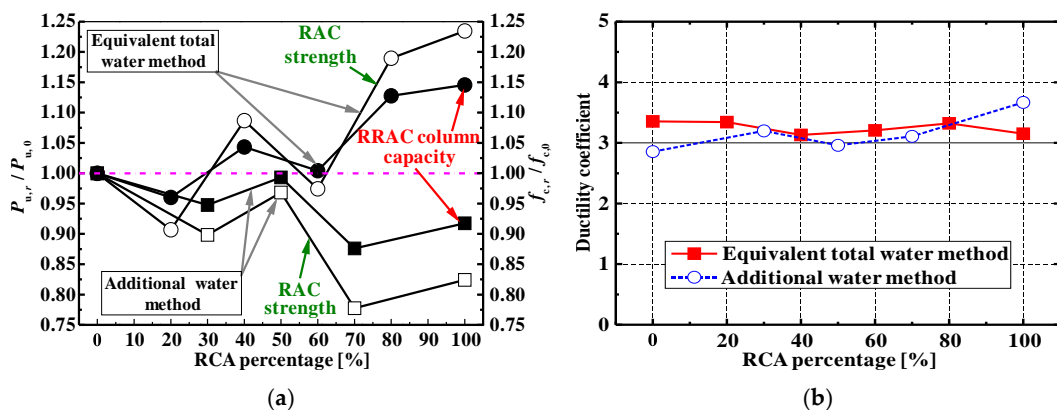


Figure 9. Effect of RCA percentage on seismic performance of RRC columns (Note: $P_{c,0}$ is the ultimate lateral load when $r = 0\%$; $P_{c,r}$ is the ultimate lateral load when $r \neq 0\%$). (a) Capacity. (b) Ductility.

Due to the relatively pronounced and interesting effects caused by using the AWM, the numerical study in the following sections was based on the specimens (NAC-0.30-60, RAC50-0.30-60, and RAC100-0.30-60) reported in Yang [43], where the AWM was adopted.

3.2. Influences of f_y and ρ_s

Four classes of steel reinforcement in accordance with the Chinese concrete design code (GB 50010-2010 [78]) were employed to conduct the parametric study. The values of steel yield strength f_y corresponding to the four classes were 300, 335, 400, and 500 MPa. The elastic modulus of the steel reinforcement E_s was taken as 200 GPa. The numerical models of RRC columns in this section were established based on the specimens reported in Yang [43] via varying the values of f_y described above.

Figure 10 illustrates the calculated hysteresis loops for the RRC columns, and Figure 11 shows the seismic performance indexes (i.e., P_u and μ) of those columns. From Figures 10 and 11 it can be concluded that improving f_y definitely resulted in a marked increase in P_u . But increasing f_y also reduced the ductility of RRC columns. This reduction can be explained by the inconsistent increase in the yield displacement (i.e., Δ_y) and the ultimate displacement (i.e., $\Delta_{0.85}$) when higher-strength steel was used. The former (Δ_y) was increased more significantly than the latter ($\Delta_{0.85}$), thus reducing the ductility ratio, as defined in Equation (5).

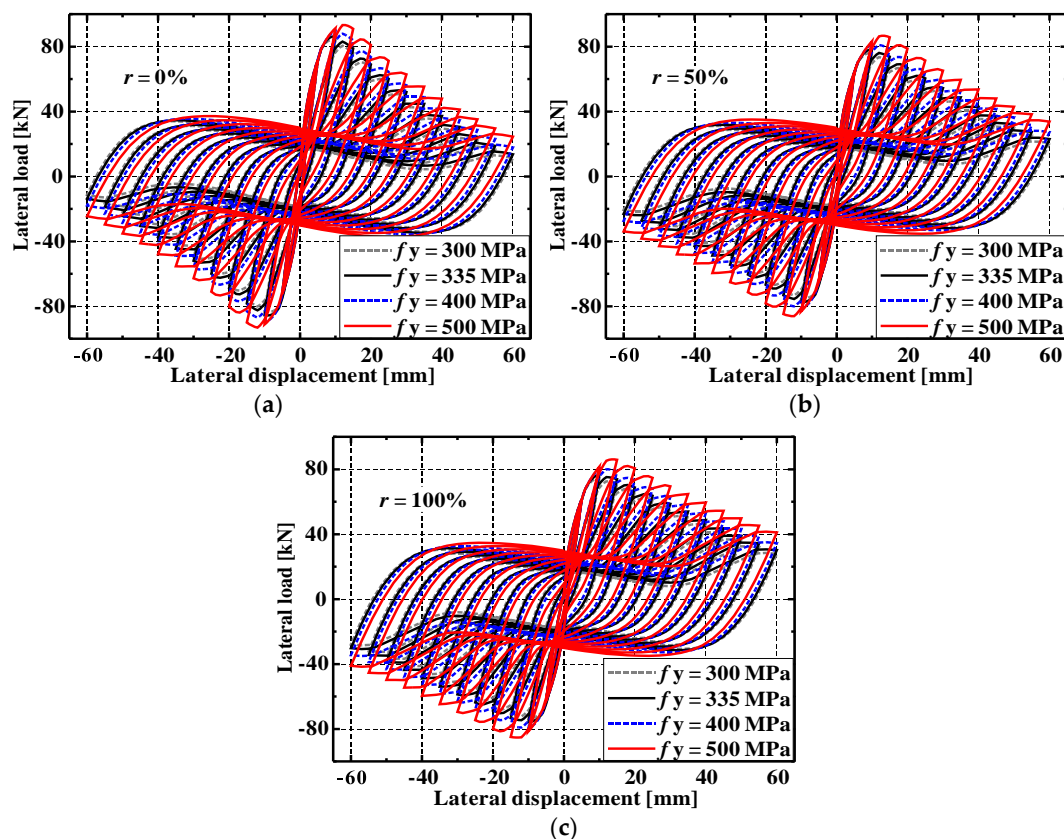


Figure 10. Effect of steel yield strength on hysteresis loops of RRC columns ($n = 0.3$). (a) $r = 0\%$, (b) $r = 50\%$, and (c) $r = 100\%$.

From Figure 10a, it was also noticed that the value of P_u at a specific yield strength (f_y) generally decreased with an increase in r because the AWM was adopted as discussed in Section 3.1. It should be highlighted that a similar study on the axial load capacity of RRC columns manufactured using the ETWM have been reported in the previous investigation conducted by authors (i.e., [64]), showing that the ETWM generally leads to a slight increase in the load capacity as a function of r .

The influence of area ratio of steel reinforcement ($\rho_s = A_s/A$) on the seismic performance of RRC columns was also discussed. The values of $\rho_s = 1.57\%$, 2.79% , 4.36% , or 6.28% were considered by varying the diameter of the longitudinal steel reinforcement (i.e., $d = 12, 16, 20$, and 24 mm).

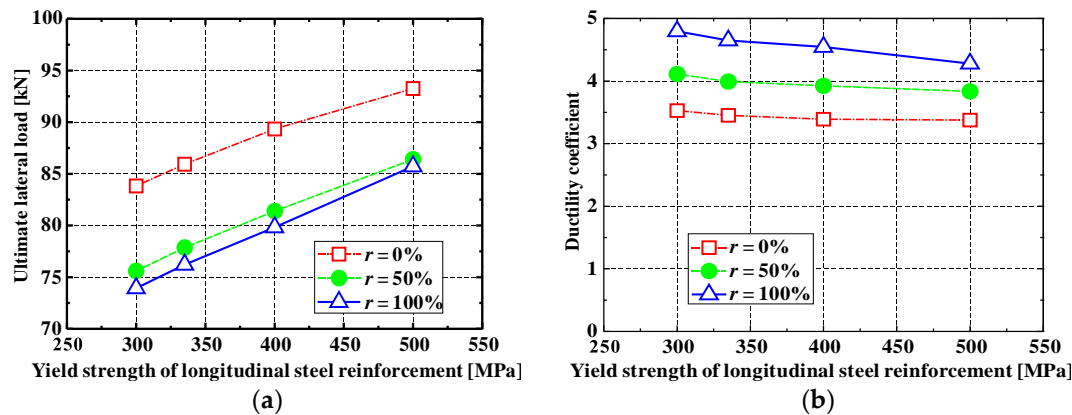


Figure 11. Effect of steel yield strength on seismic performance of RRC columns. (a) Capacity. (b) Ductility.

Figure 12 shows the hysteresis loops of RRC columns with different ρ_s . Figure 13 shows the influence of ρ_s on the seismic performance indexes. As expected, an increase in ρ_s resulted in a substantial increase in P_u . This was because the steel reinforcement ratio contributed significantly in the flexural strength of the members. On the other hand, an increase in ρ_s resulted in a reduction in μ of RRC columns. In fact, the ductility characteristic was not only affected by concrete but also related to the stress level in the longitudinal bars caused by the axial compressive load; the following derivation clearly shows this.

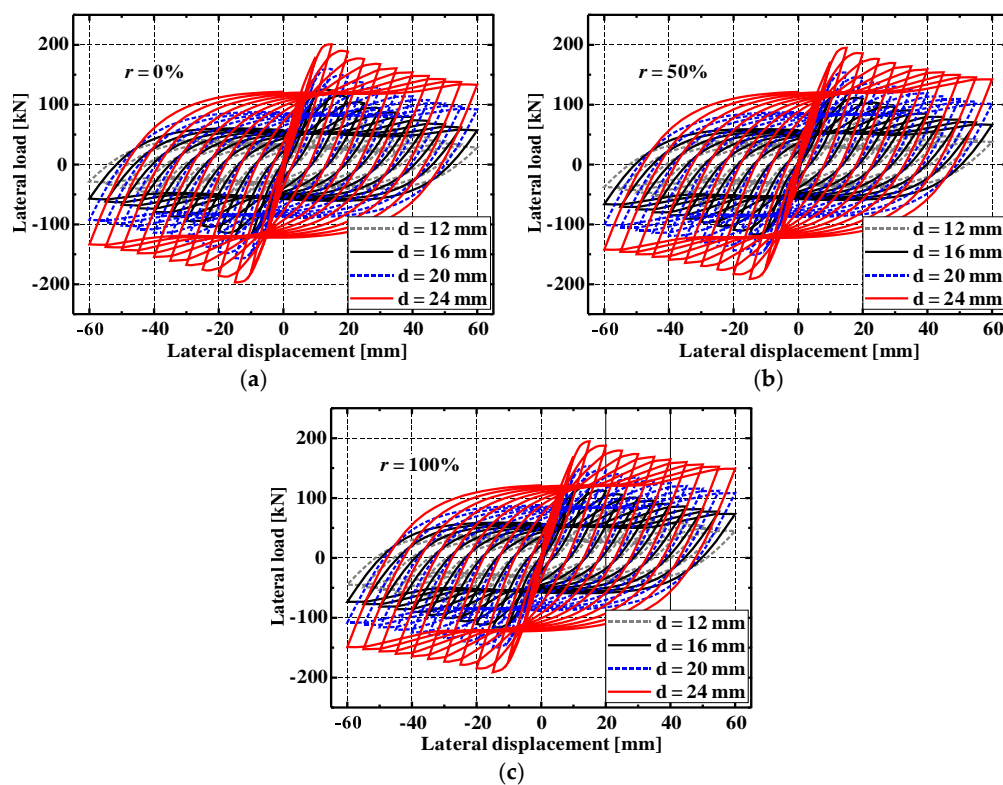


Figure 12. Effect of steel ratio on hysteresis loops of RRC columns ($n = 0.3$). (a) $r = 0\%$, (b) $r = 50\%$, and (c) $r = 100\%$.

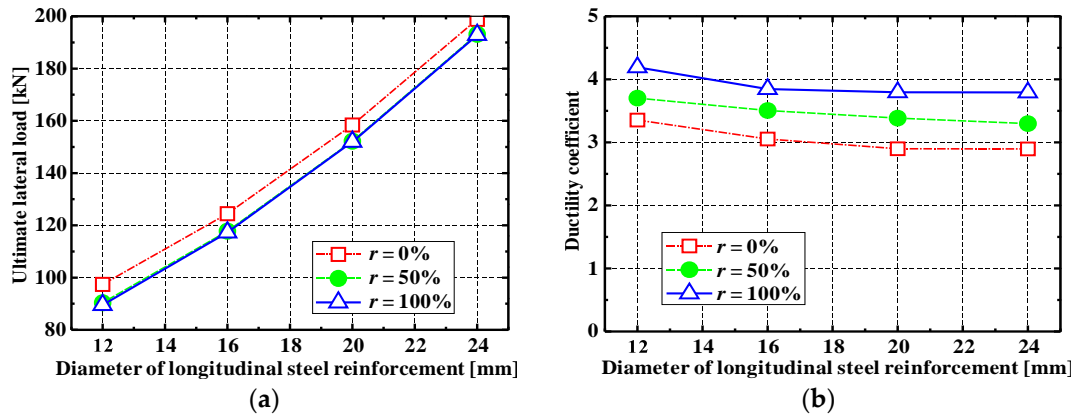


Figure 13. Effect of steel ratio on the seismic performance of RRC columns. (a) Capacity. (b) Ductility.

The strain compatibility can be assumed between concrete and longitudinal steel reinforcement, leading to:

$$\varepsilon_c = \varepsilon_s \rightarrow \frac{\sigma_c}{E_c} = \frac{\sigma_s}{E_s} \rightarrow \sigma_c = \frac{E_c}{E_s} \sigma_s = \alpha_{cs} \sigma_s, \quad (6)$$

where ε_c and ε_s are the strain of concrete and longitudinal steel reinforcement, respectively; σ_c and σ_s are the stress of concrete and longitudinal bars, respectively; E_c and E_s are the elastic modulus of concrete and steel, respectively; and α_{cs} is equal to the ratio of E_c/E_s .

A relationship between the axial load ratio and the stress level of longitudinal bars can be obtained:

$$n = \frac{N}{f_{cp} A} = \frac{\sigma_c A_c + \sigma_s A_s}{f_{cp} A} = \frac{\alpha_{cs} \sigma_s (A - A_s) + \sigma_s A_s}{f_{cp} A} = \frac{\sigma_s [\alpha_{cs} A + (1 - \alpha_{cs}) A_s]}{f_{cp} A} \quad (7)$$

$$\sigma_s = \frac{n f_{cp} A}{\alpha_{cs} A + (1 - \alpha_{cs}) A_s} \Rightarrow \frac{n f_{cp} A}{\alpha_{cs} A + (1 - \alpha_{cs}) A_s} \boxed{A_s \uparrow} = \boxed{\sigma_s \downarrow}$$

where A_c and A_s are the sectional area of concrete and longitudinal bars, respectively; and $A = A_c + A_s$.

It can be seen from Equation (7) that given a certain axial load ratio and strength class of concrete, increasing the steel ratio (ρ_s) led to a decrease in the stress level of steel reinforcement. Consequently, more stress would be transferred and sustained by the concrete, which accelerated its damage in cyclic loading. The ductility of RRC columns thus decreased with increasing the area ratio of steel reinforcement.

3.3. Influence of Bi-Directional Loading

RC structures are often subjected to multi-directional loadings under earthquake ground motions [79,80]. A bi-directional loading scheme was used herein to investigate the seismic performance of RRC columns. Figure 14 shows the definition of loading angle (α) of P to P_x , in which $P = (P_x^2 + P_y^2)^{0.5}$ is the resultant force, and P_x and P_y are the components in X and Y directions, respectively. Loading angles of 0° and 45° were employed to study the impact of bi-directional loading on the seismic performance of RRC columns.

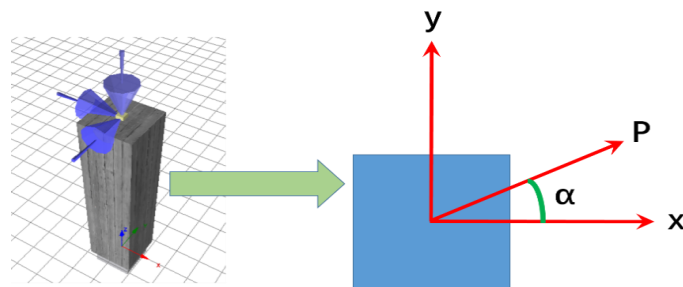


Figure 14. Lateral bi-directional loading for RRC columns.

Figure 15 shows the hysteresis loops of RRC columns with different values of α , and the influences of α on P_u and μ are plotted in Figure 16. Remarkable findings can be observed from Figures 15 and 16: (1) α had no remarkable influence on the initial stiffness of RRC columns, (2) P_u of RRC columns subjected to the loading angle of 45° was lower than that of RRC columns with a 0° loading angle, and (3) μ of RRC columns with the loading angle of 45° was larger than that of RRC columns with 0° . The reason was that the bi-directional loading scheme resulted in the coupling behavior of RC columns—that is, one direction loading can weaken the load-carrying capacity in another direction. On the contrary, one direction loading can expedite the lateral deformation in another direction.

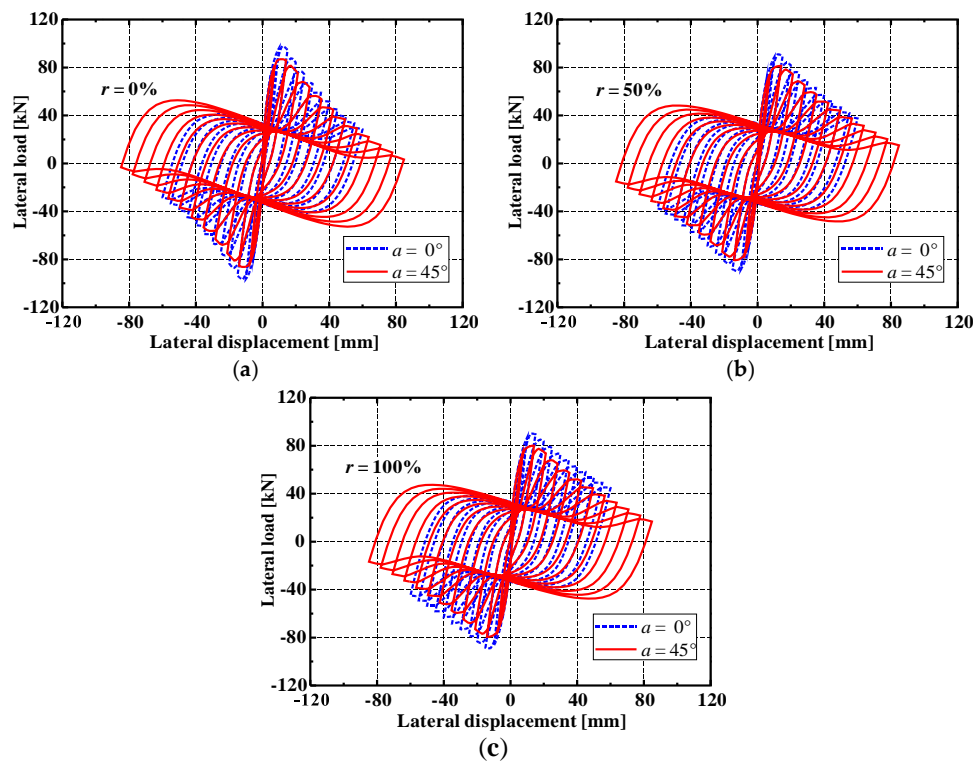


Figure 15. Effect of bi-directional loading on hysteresis loops of RRC columns ($n = 0.3$). (a) $r = 0\%$, (b) $r = 50\%$, and (c) $r = 100\%$.

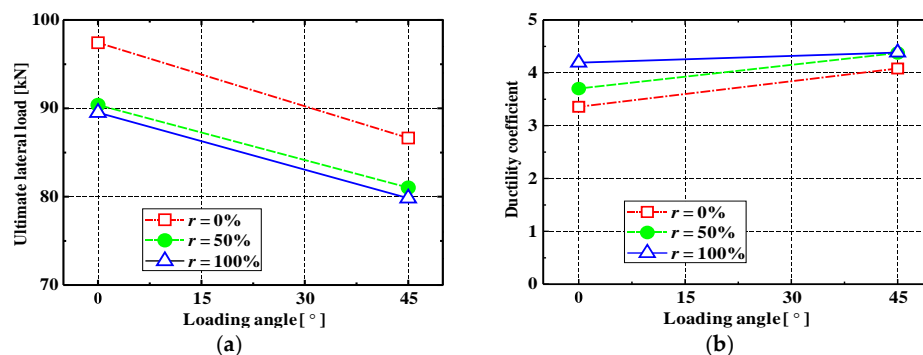


Figure 16. Effect of bi-directional loading on the seismic performance of RRC columns. (a) Capacity. (b) Ductility.

4. Grey Relational Analysis (GRA)

In addition to the numerical model, grey relational analysis (GRA) was also presented in this study to further evaluate the variable sensitivity of the seismic performance of RRC columns. As a set of system theory, grey relational model is a mathematics-based approach to compute the degrees of the correlation between the independent variables (IVs) and dependent variables (DVs) (i.e., [81,82]). Many

investigation efforts (i.e., [83–86]) have demonstrated that GRA was an effective solution to optimize the engineering materials and structures showing the level of influence of each variable involved in the problem. Based on the experimental dataset collected from Xiao et al. [42] and Yang [43], GRA was employed to determine the effects of material strengths, geometry dimensions, reinforcement configurations, axial load ratios, and RCA percentages on the hysteretic performance of RRC columns.

4.1. Mathematical Model of GRA

The maximum load (P_u) and the displacement ductility coefficient (μ) reported in Xiao et al. [42] and Yang [43] were determined as the reference matrix, $X_0(j)$, where, $j = 1, 2, \dots, n$. The key experimental parametric variables, including $r, f_y, L/h, \rho_s$ and n , were selected as the comparative matrix, $X_i(j)$, where, $i = 1, 2, \dots, m$. The following equation is a mathematical model for the construction of the reference matrix and the comparative matrix.

$$\begin{aligned} X_0 &= X_0(1), X_0(2), \dots, X_0(n) \\ X_1 &= X_1(1), X_1(2), \dots, X_1(n) \\ &\dots \\ X_m &= X_m(1), X_m(2), \dots, X_m(n) \end{aligned} \quad (8)$$

Normalization of variables in the matrix is processed in order to eliminate their numerical fluctuation.

$$x_i(j) = \frac{X_i(j)}{\frac{1}{n} \sum_{i=1}^n X_i(j)}. \quad (9)$$

The grey relational coefficient ξ_i is calculated:

$$\xi_i[x_0(j), x_i(j)] = \left| \frac{\min_{i=1,n} \min_{j=1,m} \Delta_i(j) + \rho \max_{i=1,n} \max_{j=1,m} \Delta_i(j)}{\Delta_i + \rho \max_{i=1,n} \max_{j=1,m} \Delta_i(j)} \right|, \quad (10)$$

$$\Delta_i(j) = |x_0(j) - x_i(j)|, \quad (11)$$

$$\min_{i=1,n} \min_{j=1,m} \Delta_i(j) = \max_i \left(\max_j |x_0(j) - x_i(j)| \right), \quad (12)$$

$$\max_{i=1,n} \max_{j=1,m} \Delta_i(j) = \min_i \left(\min_j |x_0(j) - x_i(j)| \right), \quad (13)$$

where $0 \leq \rho \leq 1$, and its frequently-used value is equal to 0.5 [81].

In GRA, grey relational entropy density (γ) can be used to measure the degree of correlation between the reference matrix and the comparative matrix:

$$\gamma = \frac{1}{n} \sum_{i=1}^n \xi_i[x_0(j), x_i(j)] \leq 1.0. \quad (14)$$

It is worth noting that values of γ approaching the unit indicates a closer correlation between the IVs and the DVs; when γ is over 0.7, there is a strong correlation between the IVs and the DVs; when γ is less than 0.5, the correlation between the IVs and the DVs can be considered negligible [81].

4.2. Evaluation of Variable Sensitivity

Table 2 shows the results of the grey relational evaluation between hysteretic performance and parameters. From Table 2, it can be seen that:

- (i) for the maximum lateral load P_u , the influencing sequence was: $L/h > \rho_s = f_y = n > r$;
- (ii) for the displacement ductility μ , the influencing sequence was: $L/h > \rho_s = f_y > n > r$.

Table 2. Ranking results of grey relational evaluation.

Performance	Grey Relational Entropy Density γ_i				
	r	L/h	f_y	ρ_s	n
P_u	0.62	0.87	0.86	0.86	0.85
μ	0.58	0.84	0.83	0.83	0.80

Observations from Table 2 are summarized as:

- (1) The steel strength (i.e., f_y), the geometric ratio (i.e., L/h), the reinforcement area ratio (i.e., ρ_s), and the axial load ratio (n) had the most significant influences on the seismic performance of RRC columns, with γ ranging from 0.80 to 0.87;
- (2) The sensitivity of RCA percentage on the seismic performance of RRC columns was much less remarkable than that of the steel strength and the other three structural factors (i.e., L/h , ρ_s , and n); however, considering that concrete constituted a large portion of the overall resistance, the influence of RCA percentage should be considered in the seismic design and evaluation of RRC columns.

5. Conclusions

Previous studies on evaluating the seismic performance of concrete columns made with RCAs are still not often seen. These columns have many potential applications in areas with seismic design requirements. With the aim of addressing this significant gap, this research presents a simple, yet practical and efficient, numerical method implemented in the SeismoStruct software to provide an in-depth understanding of the seismic performance of RRC columns. The findings from this study support the following conclusions:

- (1) The lateral load-carrying capacity of RRC columns using the AWM generally reduces (up to 10%) with an increase in the RCA replacement percentage, whilst this trend is reversed when the ETWM is used.
- (2) Increasing the steel strength is advantageous to the gain in lateral strength of the RRC column, but this leads to a reduction in ductility. Similar two-edged results are also observed when increasing the area ratio of steel reinforcement.
- (3) Bi-directional loading has a negative influence on the lateral load-carrying capacity, but it has a positive influence on the ductility of RRC columns.
- (4) The steel strength and some well-recognized structural factors (i.e., the shear-span ratio, the area ratio of steel reinforcement, and the axial load ratio) are identified by the GRA method as the most essential parameters affecting the seismic performances of RRC columns, with the grey relational entropy density, γ , ranging from 0.80 to 0.87.
- (5) The sensitivity of RCA percentage on the seismic performance of RRC columns is quite modest compared to those of the four factors listed in (4); however, quality and percentage of RAC still should be well-controlled in seismic design of RRC columns.

Overall, it can be said that the use of the RRC columns in seismic regions is generally viable. Those green columns can be properly seismically designed with confidence despite some of the deleterious aspects. However, further studies are still needed, such as determining the minimum longitudinal and transverse steel ratios used in RRC columns, to suppress any negative effects caused by the incorporation of RAC. More experimental data are also called for to investigate the variability of the seismic performance of RRC columns and, finally, to determine their seismic reliability.

Author Contributions: X.-Y.Z., J.-J.X., and F.W. performed the numerical analysis and wrote the whole paper; Y.Y., T.-Y.X., and S.T.D. revised the paper.

Funding: The authors would like to gratefully acknowledge research grants from the National Natural Science Foundation of China (Project Nos: 51708289 and 51608435), Postdoctoral Science Foundation of China (Project No: 2017M611796), Fund of State Key Laboratory of Subtropical Building Science of China (Project Nos: 2017KC18, 2018ZB34 and 2019ZB22), Special Fund for Energy Conservation of Guangzhou (Project No: J-2016-01) and Fundamental Research Fund for the Central Universities (Project No: 2018ZD43).

Conflicts of Interest: The authors declare that there is no conflict of interest regarding the publication of this paper.

Abbreviations

A	Column sectional area
A_c	Concrete sectional area
A_s	Total sectional area of longitudinal rebars
b	Column sectional width
D_c	Diameter of concrete cylinder
d	Diameter of longitudinal rebar
d_{hoop}	Diameter of transverse rebar
E_c	Elastic modulus of concrete
E_s	Elastic modulus of longitudinal rebar
f_c	Concrete cylindrical compressive strength
f_y	Yield strength of longitudinal rebar
$f_{y,v}$	Yield strength of transverse rebar
h	Column sectional height
H_c	Height of concrete cylinder
L	Column effective length
N	Axial load
n	Axial load ratio
P	Lateral load
r	Replacement ratio of RCAs [%]
S	Hoop spacing
w_{eff}/c	Effective water to cement ratio
w_d	Coefficient accounting for concrete density
w_s	Coefficient considering sample aspect ratio
w_a	Coefficient considering sample aspect ratio
σ_c	Stress of concrete
σ_s	Stress of longitudinal bar
ε_{cor}	Peak strain of RAC
ε_c	Strain of concrete
ε_s	Strain of longitudinal rebar
ε_{con}	Peak strain of NAC
$\rho_{c,f}$	Bulk density of concrete
ρ_s	Area ratio of steel rebar
ζ_i	Grey correlation coefficient
γ_i	Grey correlation entropy density
α	Bi-directional cyclic loading angle
μ	Displacement ductility coefficient
$\Delta_{0.85}$	Lateral displacement at 85% peak load
Δ_y	Yield lateral displacement

References

1. Loo, Y.H.; Tam, C.T.; Ravindrarajah, R.S. Recycled concrete as fine and coarse aggregate in concrete. *Mag. Concr. Res.* **1987**, *39*, 214–220.
2. Pacheco, J.; de Brito, J.; Chastre, C.; Evangelista, L. Uncertainty models of reinforced concrete beams in bending: Code comparison and recycled aggregate incorporation. *J. Strut. Eng.* **2019**, *145*, 04019013. [[CrossRef](#)]

3. Pepe, M.; Filho, R.D.T.; Koenders, E.A.B.; Martinelli, E. A novel mix design methodology for recycled aggregate concrete. *Constr. Build. Mater.* **2016**, *122*, 362–372. [\[CrossRef\]](#)
4. Fathifazl, G.; Abbas, A.; Razaqpur, A.G.; Isgor, O.B.; Fournier, B.; Foo, S. New mixture proportioning method for concrete made with coarse recycled concrete aggregate. *J. Mater. Civ. Eng.* **2009**, *21*, 601–611. [\[CrossRef\]](#)
5. Matias, D.; de Brito, J.; Rosa, A.; Pedro, D. Mechanical properties of concrete produced with recycled coarse aggregates—Influence of the use of super plasticizers. *Constr. Build. Mater.* **2013**, *44*, 101–109. [\[CrossRef\]](#)
6. Ceia, F.; Raposo, J.; Guerra, M.; Júlio, E.; de Brito, J. Shear strength of recycled aggregate concrete to natural aggregate concrete interfaces. *Constr. Build. Mater.* **2016**, *109*, 139–145. [\[CrossRef\]](#)
7. Kurda, R.; de Brito, J.; Silvestre, J.D. Indirect evaluation of the compressive strength of recycled aggregate concrete with high fly ash ratios. *Mag. Concr. Res.* **2017**, *70*, 1–13. [\[CrossRef\]](#)
8. Xu, J.J.; Zhao, X.Y.; Yu, Y.; Xie, T.Y.; Yang, G.S.; Xue, J.Y. Parametric sensitivity analysis and modelling of mechanical properties of normal- and high-strength recycled aggregate concrete using grey theory, multiple nonlinear regression and artificial neural networks. *Constr. Build. Mater.* **2019**, *211*, 479–491. [\[CrossRef\]](#)
9. Thomas, C.; Setién, J.; Polanco, J.A.; Alaejos, P.; de Juan, M.S. Durability of recycled aggregate concrete. *Constr. Build. Mater.* **2013**, *40*, 1054–1065. [\[CrossRef\]](#)
10. Ozbakkaloglu, T.; Gholampour, A.; Xie, T.Y. Mechanical and durability properties of recycled aggregate concrete: Effect of recycled aggregate size and content on the behaviour. *J. Mater. Civ. Eng.* **2017**, *30*, 04017275. [\[CrossRef\]](#)
11. Han, B.C.; Yun, H.D.; Chung, S.Y. Shear capacity of reinforced concrete beams made with recycled-aggregate. *ACI Spec. Publ.* **2001**, *200*, 503–516.
12. Sogo, M.; Sogabe, T.; Maruyama, I.; Sato, R.; Kawai, K. Shear behaviour of reinforced recycled concrete beams. In Proceedings of the Conference on the Use of Recycled Materials in Building and Structures, Barcelona, Spain, 8–11 November 2004.
13. González-Fontebo, B.; Martínez-Abella, F. Shear strength of recycled concrete beams. *Constr. Build. Mater.* **2007**, *21*, 887–893. [\[CrossRef\]](#)
14. Choi, H.B.; Yi, C.K.; Cho, H.H.; Kang, K.I. Experimental study on the shear strength of recycled aggregate concrete beams. *Mag. Concr. Res.* **2010**, *62*, 103–114. [\[CrossRef\]](#)
15. Fathifazl, G.; Razaqpur, A.G.; Isgor, O.B.; Abbas, A.; Fournier, B.; Foo, S. Shear strength of reinforced recycled concrete beams without stirrups. *Mag. Concr. Res.* **2009**, *61*, 387–400. [\[CrossRef\]](#)
16. Fathifazl, G.; Razaqpur, A.G.; Isgor, O.B.; Abbas, A.; Fournier, B.; Foo, S. Shear strength of steel reinforced recycled concrete beams with stirrups. *Mag. Concr. Res.* **2010**, *62*, 685–699. [\[CrossRef\]](#)
17. Fathifazl, G.; Razaqpur, A.G.; Isgor, O.B.; Abbas, A.; Fournier, B.; Foo, S. Shear capacity evaluation of steel reinforced recycled concrete (RRC) beams. *Eng. Struct.* **2011**, *33*, 1025–1033. [\[CrossRef\]](#)
18. Arezoumandi, M.; Smith, A.; Volz, J.S.; Khayat, K.H. An experimental study on shear strength of reinforced concrete beams with 100% recycled concrete aggregate. *Constr. Build. Mater.* **2014**, *53*, 612–620. [\[CrossRef\]](#)
19. Knaack, A.M.; Kurama, Y.C. Behavior of reinforced concrete beams with recycled concrete coarse aggregates. *J. Struct. Eng.* **2015**, *141*, B4014009. [\[CrossRef\]](#)
20. Sadati, S.; Arezoumandi, M.; Khayat, K.H.; Volz, J.S. Shear performance of reinforced concrete beams incorporating recycled concrete aggregate and high-volume fly ash. *J. Clean. Prod.* **2016**, *115*, 284–293. [\[CrossRef\]](#)
21. Rahal, K.N.; Alrefaei, Y.T. Shear strength of longitudinally reinforced recycled aggregate concrete beams. *Eng. Struct.* **2017**, *145*, 273–282. [\[CrossRef\]](#)
22. Ivan, S.I.; Snežana, B.M.; Nikola, T. Shear behaviour of recycled aggregate concrete beams with and without shear reinforcement. *Eng. Struct.* **2017**, *141*, 386–401.
23. Brandes, M.R.; Kurama, Y.C. Behavior of shear-critical prestressed concrete beams with recycled concrete aggregates under ultimate loads. *Eng. Struct.* **2018**, *165*, 237–246. [\[CrossRef\]](#)
24. Sogo, M.; Sogabe, T.; Sato, R.; Kawai, K. Flexural properties of reinforced recycled concrete beams. In Proceedings of the Conference on the Use of Recycled Materials in Building and Structures, Barcelona, Spain, 8–11 November 2004.
25. Sato, R.; Maruyama, I.; Sogabe, T.; Sogo, M. Flexural behavior of reinforced recycled concrete beams. *J. Adv. Concr. Technol.* **2007**, *5*, 43–61. [\[CrossRef\]](#)
26. Fathifazl, G.; Razaqpur, A.G.; Isgor, O.B.; Abbas, A.; Fournier, B.; Foo, S. Flexural performance of steel reinforced recycled concrete (RRC) beams. *ACI Struct. J.* **2009**, *106*, 858–867.

27. Choi, W.C.; Kim, S.W.; Yun, H.D. Flexural performance of reinforced recycled aggregate concrete beams. *Mag. Concr. Res.* **2012**, *64*, 837–848. [\[CrossRef\]](#)
28. Ignjatovic, I.; Marinkovic, S.; Miškovic, Z.; Savic, A. Flexural behavior of reinforced recycled aggregate concrete beams under short-term loading. *Mater. Struct.* **2013**, *46*, 1045–1059. [\[CrossRef\]](#)
29. Disfani, M.M.; Arulrajah, A.; Haghighi, H.; Mohammadinia, A.; Horpibulsuk, S. Flexural beam fatigue strength evaluation of crushed brick as a supplementary material in cement stabilized recycled concrete aggregates. *Constr. Build. Mater.* **2014**, *68*, 667–676. [\[CrossRef\]](#)
30. Kang, T.H.K.; Kim, W.; Kwak, Y.K.; Hong, S.G. Flexural testing of reinforced concrete beams with recycled concrete aggregates (with appendix). *ACI Struct. J.* **2014**, *111*, 607–616.
31. Arezoumandi, M.; Smith, A.; Volz, J.S.; Khayat, K.H. An experimental study on flexural strength of reinforced concrete beams with 100% recycled concrete aggregate. *Eng. Struct.* **2015**, *88*, 154–162. [\[CrossRef\]](#)
32. Evangelista, L.; de Brito, J. Flexural behaviour of reinforced concrete beams made with fine recycled concrete aggregates. *KSCE J. Civ. Eng.* **2017**, *21*, 1–11. [\[CrossRef\]](#)
33. Mohammeda, T.U.; Das, H.K.; Mahmood, Z.H.; Rahman, M.N.; Awal, M.A. Flexural performance of RC beams made with recycled brick aggregate. *Constr. Build. Mater.* **2017**, *134*, 67–74. [\[CrossRef\]](#)
34. Yang, S.; Lee, H. Structural performance of reinforced RCA concrete beams made by a modified EMV method. *Sustainability* **2017**, *9*, 131. [\[CrossRef\]](#)
35. Seara-Paz, S.; González-Fontboa, B.; Martínez-Abella, F.; Eiras-López, J. Flexural performance of reinforced concrete beams made with recycled concrete coarse aggregate. *Eng. Struct.* **2018**, *156*, 32–45. [\[CrossRef\]](#)
36. Katkhuda, H.; Shatarat, N. Shear behavior of reinforced concrete beams using treated recycled concrete aggregate. *Constr. Build. Mater.* **2016**, *125*, 63–71. [\[CrossRef\]](#)
37. Ajdukiewicz, A.B.; Kliszczewicz, A.T. Comparative tests of beams and columns made of recycled aggregate concrete and natural aggregate concrete. *J. Adv. Concr. Technol.* **2007**, *5*, 259–273. [\[CrossRef\]](#)
38. Wang, Y.Y.; Chen, J.; Zong, B.; Geng, Y. Mechanical behavior of axially loaded recycled aggregate concrete filled steel tubular stubs and reinforced recycled aggregate concrete stubs. *J. Build. Struct.* **2011**, *32*, 170–177.
39. Choi, W.C.; Yun, H.D. Compressive behavior of reinforced concrete columns with recycled aggregate under uniaxial loading. *Eng. Struct.* **2012**, *41*, 285–293. [\[CrossRef\]](#)
40. Silva, R.V.; de Brito, J.; Evangelista, L.; Dhir, R.K. Design of reinforced recycled aggregate concrete elements in conformity with Eurocode 2. *Constr. Build. Mater.* **2016**, *105*, 144–156. [\[CrossRef\]](#)
41. Tošić, N.; Marinkovic, S.; Ignjatovic, I. A database on flexural and shear strength of reinforced recycled aggregate concrete beams and comparison to Eurocode 2 predictions. *Constr. Build. Mater.* **2016**, *127*, 932–944. [\[CrossRef\]](#)
42. Xiao, J.Z.; Huang, X.; Shen, L.M. Seismic behavior of semi-precast column with recycled aggregate concrete. *Constr. Build. Mater.* **2012**, *35*, 988–1001. [\[CrossRef\]](#)
43. Yang, Y.Q. *Experimental Study on Seismic Performance of Recycled Aggregate Concrete Columns*; Harbin Institute Technology: Harbin, China, 2016.
44. Xiao, J.Z.; Wang, C.Q.; Pham, T.L.; Yang, Z.J.; Ding, T. Nonlinear analysis and test validation on seismic performance of a recycled aggregate concrete space frame. *Struct. Des. Tall Spec.* **2015**, *23*, 1381–1405. [\[CrossRef\]](#)
45. SeismoSoft. SeismoStruct—A Computer Program for Static and Dynamic Nonlinear Analysis of Framed Structures. 2014. Available online: www.seismosoft.com (accessed on 20 March 2019).
46. Zhang, Y.Y.; Harries, K.A.; Yuan, W.C. Experimental and numerical investigation of the seismic performance of hollow rectangular bridge piers constructed with and without steel fiber reinforced concrete. *Eng. Struct.* **2013**, *48*, 255–265. [\[CrossRef\]](#)
47. Ahmad, S.H.; Weerakoon, S.L. Model for behavior of slender reinforced concrete columns under biaxial bending. *ACI Struct. J.* **1995**, *92*, 188–198.
48. Bahn, B.Y.; Hsu, C.T.T. Cyclically and biaxially loaded reinforced concrete slender columns. *ACI Struct. J.* **2000**, *97*, 444–454.
49. Barrera, A.C.; Bonet, J.L.; Romero, M.L.; Miguel, P.F. Experimental tests of slender reinforced concrete columns under combined axial load and lateral force. *Eng. Struct.* **2001**, *33*, 3676–3689. [\[CrossRef\]](#)
50. Barrera, A.C.; Bonet, J.L.; Romero, M.L.; Fernández, M.A. Ductility of slender reinforced concrete columns under monotonic flexural and constant axial load. *Eng. Struct.* **2012**, *40*, 398–412. [\[CrossRef\]](#)

51. Babazadeh, A.; Burgueño, R.; Silva, P.F. Evaluation of the critical plastic region length in slender reinforced concrete bridge columns. *Eng. Struct.* **2016**, *125*, 280–293. [[CrossRef](#)]
52. Madas, P. *Advanced Modelling of Composite Frames Subjected to Earthquake Loading*; Imperial College, University of London: London, UK, 1993.
53. Mander, J.B.; Priestley, M.J.N.; Park, R. Theoretical stress–strain model for confined concrete. *J. Struct. Eng.* **1998**, *114*, 1804–1826. [[CrossRef](#)]
54. Martinez, R.J.E.; Elnashai, A.S. Confined concrete model under cyclic load. *Mater. Struct.* **1997**, *30*, 139–147. [[CrossRef](#)]
55. Gholampour, A.; Gandomi, A.H.; Ozbakkaloglu, T. New formulations for mechanical properties of recycled aggregate concrete using gene expression programming. *Constr. Build. Mater.* **2017**, *130*, 122–145. [[CrossRef](#)]
56. Xiao, J.Z.; Li, J.B.; Zhang, C. Mechanical properties of recycled aggregate concrete under uniaxial loading. *Cement Concr. Res.* **2005**, *35*, 1187–1194. [[CrossRef](#)]
57. Lim, J.C.; Ozbakkaloglu, T. Stress-strain model for normal- and light-weight concretes under uniaxial and triaxial compression. *Constr. Build. Mater.* **2014**, *71*, 492–509. [[CrossRef](#)]
58. Yassin, M.H.M. *Nonlinear Analysis of Prestressed Concrete Structures under Monotonic and Cyclic Loads*; University of California: Berkeley, CA, USA, 1994.
59. Menegotto, M.; Pinto, P.E. Method of analysis for cyclically loaded R.C. plane frames including changes in geometry and non-elastic behaviour of elements under combined normal force and bending. In *Symposium on the Resistance and Ultimate Deformability of Structures Acted on by Well Defined Repeated Loads*; International Association for Bridge and Structural Engineering: Zurich, Switzerland, 1973.
60. Filippou, F.C.; Popov, E.P.; Bertero, V.V. *Effects of Bond Deterioration on Hysteretic Behaviour of Reinforced Concrete Joints*; Report EERC 83-19; Earthquake Engineering Research Center, University of California: Berkeley, CA, USA, 1983.
61. Monti, G.; Nuti, C.; Santini, S. CYRUS—Cyclic Response of Upgraded Sections; Report No. 96-2; University of Chieti: Chieti, Italy, 1996.
62. Ferreira, L.; de Brito, J.; Barra, M. Influence of the pre-saturation of recycled coarse concrete aggregates on concrete properties. *Mag. Concr. Res.* **2011**, *63*, 617–627. [[CrossRef](#)]
63. González-Taboada, I. *Self-Compacting Recycled Concrete: Basic Mechanical Properties, Rheology, Robustness and Thixotropy*; Universidade da Coruña: A Coruña, Spain, 2016.
64. Xu, J.J.; Chen, Z.P.; Ozbakkaloglu, T.; Zhao, X.Y.; Demartino, C. A critical assessment of the compressive behavior of reinforced recycled aggregate concrete columns. *Eng. Struct.* **2018**, *161*, 161–175. [[CrossRef](#)]
65. González-Fontebo, B.; Martínez-Abella, F.; Carro, L.D.; Seara-Paz, S. Stress-strain relationship in axial compression for concrete using recycled saturated coarse aggregate. *Constr. Build. Mater.* **2011**, *25*, 2335–2342.
66. Silva, R.V.; de Brito, J.; Dhir, R.K. The influence of the use of recycled aggregates on the compressive strength of concrete: A review. *Eur. J. Environ. Civ. Eng.* **2015**, *19*, 825–849. [[CrossRef](#)]
67. Pedro, D.; de Brito, J.; Evangelista, L. Performance of concrete made with aggregates recycled from precasting industry waste: Influence of the crushing process. *Mater. Struct.* **2015**, *48*, 3965–3978. [[CrossRef](#)]
68. Xu, J.J.; Chen, Z.P.; Xiao, Y.; Demartino, C.; Wang, J.H. Recycled aggregate concrete in FRP-confined columns: A review of experimental results. *Compos. Struct.* **2017**, *174*, 277–291. [[CrossRef](#)]
69. Chen, G.M.; He, Y.H.; Jiang, T.; Lin, C.J. Behavior of CFRP-confined recycled aggregate concrete under axial compression. *Constr. Build. Mater.* **2016**, *111*, 85–97. [[CrossRef](#)]
70. Teng, J.G.; Zhao, J.L.; Yu, T.; Li, L.J.; Guo, Y.C. Behavior of FRP-confined compound concrete containing recycled concrete lumps. *J. Compos. Constr.* **2016**, *20*, 04015038. [[CrossRef](#)]
71. Xu, J.J.; Chen, Z.P.; Xue, J.Y.; Chen, Y.L.; Zhang, J.T. Simulation of seismic behavior of square recycled aggregate concrete-filled steel tubular columns. *Constr. Build. Mater.* **2017**, *149*, 553–566. [[CrossRef](#)]
72. Chen, Z.P.; Xu, J.J.; Chen, Y.L.; Lui, E.M. Recycling and reuse of construction and demolition waste in concrete-filled steel tubes: A review. *Constr. Build. Mater.* **2016**, *126*, 641–660. [[CrossRef](#)]
73. Chen, Z.P.; Xu, J.J.; Xue, J.Y.; Su, Y.S. Performance and calculations of recycled aggregate concrete-filled steel tubular (RACFST) short columns under axial compression. *Int. J. Steel Struct.* **2014**, *14*, 31–42. [[CrossRef](#)]
74. Zhao, X.Y.; Wu, B.; Wang, L. Structural response of thin-walled circular steel tubular columns filled with demolished concrete lumps and fresh concrete. *Constr. Build. Mater.* **2016**, *129*, 216–242. [[CrossRef](#)]

75. Wu, B.; Peng, C.W.; Zhao, X.Y.; Zhou, W.J. Axial loading tests of thin-walled circular steel tubes infilled with cast-in-place concrete and precast segments containing DCLs. *Thin Wall Struct.* **2018**, *127*, 275–289. [[CrossRef](#)]
76. Zega, C.J.; Maio, A.A.D. Recycled concretes made with waste ready-mix concrete as coarse aggregate. *J. Mater. Civ. Eng.* **2011**, *23*, 281–286. [[CrossRef](#)]
77. Gettu, R.; Bazant, Z.P.; Karr, M.E. Fracture properties and brittleness of high-strength concrete. *ACI Mater. J.* **1990**, *87*, 608–618.
78. China Standards Publication. *Code for Design of Concrete Structures*; GB 50010-2010; China Planning Press: Beijing, China, 2010. (In Chinese)
79. Tseng, C.C.; Hwang, S.J.; Mo, Y.L.; Yeh, Y.K.; Lee, Y.T. Experiment of torsionally-coupled RC building subjected to bi-directional cyclic loading. In Proceedings of the 3rd International Conference on Advances in Experimental Structural Engineering, San Francisco, CA, USA, 15–16 October 2009.
80. Mo, Y.L.; Luu, C.H.; Nie, X.; Tseng, C.C.; Hwang, S.J. Seismic performance of a two-story unsymmetrical reinforced concrete building under reversed cyclic bi-directional loading. *Eng. Struct.* **2017**, *145*, 333–347. [[CrossRef](#)]
81. Liu, S.F.; Yang, Y.J.; Forrest, J. *Grey Data Analysis: Methods, Models and Applications*; Springer: Singapore, 2017.
82. Patton, M.Q. *Qualitative Evaluation and Research Methods*; Sage Publications: Thousand Oaks, CA, USA, 1990.
83. Zhang, Y.J.; Zhang, X. Grey correlation analysis between strength of slag cement and particle fractions of slag powder. *Cem. Concr. Compos.* **2007**, *29*, 498–504. [[CrossRef](#)]
84. Ho, P.H.K. Forecasting construction manpower demand by gray model. *J. Constr. Eng. Mag.* **2010**, *136*, 1299–1305. [[CrossRef](#)]
85. Lai, W.C.; Chang, T.P.; Wang, J.J.; Kan, C.W.; Chen, W.W. An evaluation of mahalanobis distance and grey relational analysis for crack pattern in concrete structures. *Comp. Mater. Sci.* **2012**, *65*, 115–121. [[CrossRef](#)]
86. Wang, Z.J.; Wang, Q.; Ai, T. Comparative study on effects of binders and curing ages on properties of cement emulsified asphalt mixture using gray correlation entropy analysis. *Constr. Build. Mater.* **2014**, *54*, 615–622. [[CrossRef](#)]



© 2019 by the authors. Licensee MDPI, Basel, Switzerland. This article is an open access article distributed under the terms and conditions of the Creative Commons Attribution (CC BY) license (<http://creativecommons.org/licenses/by/4.0/>).